Proceedings of Global Power and Propulsion Society
ISSN-Nr: 2504-4400
GPPS Hong Kong 2023
October 17-19, 2023
www.gpps.global

GPPS-TC-2023-0197

Direct Multi-Fidelity Integration of 3D CFD Models in a Gas Turbine with Fully Coupled Zooming Method

Weimin Deng
Southern University of Science and Technology
11930708@mail.sustech.edu.cn
Shenzhen, Guangdong, China

Zuojun Wei
Southern University of Science and Technology
stiven_wei@yahoo.com
Shenzhen, Guangdong, China

Ming Ni
Southern University of Science and Technology
nim2019@mail.sustech.edu.cn
Shenzhen, Guangdong, China

Haotian Gao
Southern University of Science and Technology
12232453@mail.sustech.edu.cnl
Shenzhen, Guangdong, China

Guangming Ren
Southern University of Science and Technology
rengm@sustech.edu.cn
Shenzhen, Guangdong, China

ABSTRACT

Multi-fidelity simulation improves the simulation accuracy and captures more detailed information about aero engines under limited computing resources, which is implemented by coupling different levels of modeling and simulation with numerical zooming methods. However, there is an obvious problem in traditional zooming methods such as the iterative coupled zooming method or mini-map method that both the convergence and accuracy are highly dependent on the component general characteristic maps. Based on the investigation of a micro gas turbine, a direct and accurate fully coupled zooming method is developed, which directly embeds the 3D CFD compressor and turbine model into a 0D component-level model without component general characteristics maps. Then, the fully coupled zooming method is compared with the traditional 0D component-level model methods in terms of the throttle characteristics of the micro gas turbine, and the experimental data of the ground test is performed to verify the effectiveness of the fully coupled zooming methods. The results indicate that the fully coupled zooming method matches well with the test data than traditional 0D component-level model methods.

Keywords: Multi-fidelity; Fully coupled; Numerical zooming method; Component level model

INTRODUCTION

Numerical zooming is a computational approach used in aeroengine design and analysis to study the flow characteristics in specific regions of interest within the engine(Jia and Tang et al., 2022; Xu and Yan et al., 2022; Yang and Wu et al., 2022; ZHENG and ZENG et al., 2023). The fully coupled method in numerical zooming involves integrating multiple modeling methods of varying fidelity and complexity into a full engine simulation. This approach is particularly useful in regions of high aerodynamic loading, such as compressor and turbine, where the flow is complex and can significantly affect engine performance(Pachidis and Pilidis et al., 2006; Pachidis and Pilidis et al., 2007; Pachidis and Pilidis et al., 2007; Klein and Reitenbach et al., 2017; Briones and Caswell et al., 2021). By coupling 3D CFD models of these regions, the fully coupled method can obtain more accurate information and better understand the impact of design changes on engine performance. Overall, the fully coupled method in numerical zooming is powerful in aeroengine design and analysis, allowing for a more comprehensive understanding of the complex flow characteristics occurring within the engine(Lytle, 2006; Schlu Ter and Apte et al., 2006; Bala, 2007; Medic and You et al., 2007; Pachidis and Pilidis et al., 2007).

The component-level models are conventionally used in simulating the overall performance of gas turbines due to their fast computational speed and simple implementation. However, their precision primarily dependent on characteristic maps and falls short in capturing detailed information of component(ZHOU and LU et al., 2019; Pang and Li et al., 2020; JIA and CHEN et al., 2021; Hao and Sun et al., 2022; Wang and Zhang et al., 2023; Zhuang and Xu et al., 2023). In order to incorporate high fidelity into the component-level model and eliminate the reliance on characteristic maps, the fully coupled zooming method has emerged as an extensively researched avenue.

The fully coupled zooming method directly embeds the CFD models into the CLM cycle. Research on the fully coupled method embedding the 1D inlet and nozzle CFD models was first conducted. The fully coupled method, which

incorporates 1D inlet and nozzle CFD models, was initially the subject of research. Connolly utilized this approach to investigate the dynamic response of engine thrust (Connolly and Friedlander et al., 2014), while Allison analyzed the impact of different attack angles on engine installation performance at supersonic speeds by embedding a 1D intake model into the entire engine CLM cycle (Allison and Alyanak, 2014). In summary, these efforts yielded improvements in simulation accuracy and the capture of detailed flow fields. However, it's worth noting that the application of fully coupled zooming methods has predominantly centered on non-rotating components, with limited attention to the high-fidelity integration of rotating components.

Unfortunately, embedding 3D CFD rotating component models in the fully coupled zooming method presents a significant challenge due to convergence issues. To address this, Fu incorporated a high-fidelity model of a non-rotating component into the CLM of a variable cycle engine model (Fu and Li et al., 2021), while Pilet added an interface between mass flow and static pressure to integrate the fully coupled zooming method into a CLM with only the 3D CFD model of a rotating fan (Pilet and Lecordix et al., 2011). Despite these endeavors, the incorporation of multiple 3D CFD rotating component models, such as those of compressors and turbines, remains a formidable challenge. Simulations often focus on the design point or a few off-design points near it, and typically involve the coupling of a single rotating component. Consequently, extending the applicability of fully coupled zooming methods to encompass multiple rotating components and broader operational ranges in complex engines poses a significant challenge.

To address these challenges, the present study proposes a fully coupled zooming method coupled compressor and turbine with high simulation accuracy. The proposed fully coupled zooming method is implemented by embedding the multiple 3D CFD models of compressor and turbine (coaxial rotating), rather than the corresponding characteristic maps, into the CLM cycle of a gas turbine. The method is used to simulate the overall performance of a KJ66 gas turbine over a wide range of off-design points. The method is compared with the traditional CLM method, and the experimental data of a ground test is used to verify its effectiveness. Overall, its applications to industry seems to be promising. The proposed method, in fact, allows to know more detailed information of flow characteristics in an engine, improving the accuracy of data, without the need to correlate data and using characteristic maps.

METHODOLOGY

Research objects

The KJ66 micro gas turbine (MGT) has gained a reputation as a mature commercial engine, with publicly available data that provide useful insights for researchers. Its dimensions are noteworthy, with a diameter of around 110 mm, a length of about 240 mm, and a total weight of approximately 0.93 kg. This engine is capable of producing a maximum thrust of 84.5 N, and it consists of three key components: a centrifugal compressor, an axial turbine, and a burner. The schematic diagram of the KJ66 MGT engine structure is depicted in Figure 1.

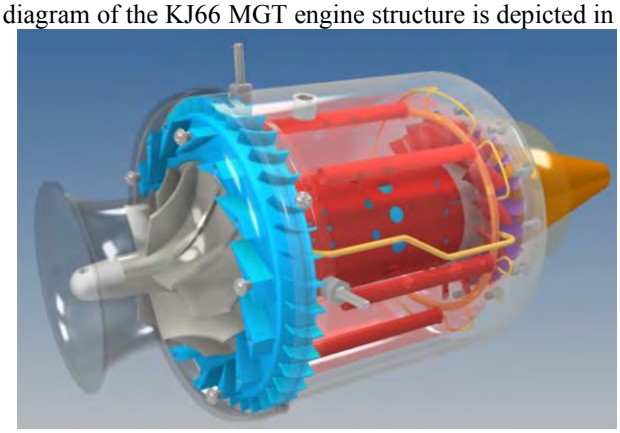

Turbine engine KJ-66 (GrabCAD)

a） schematic diagram

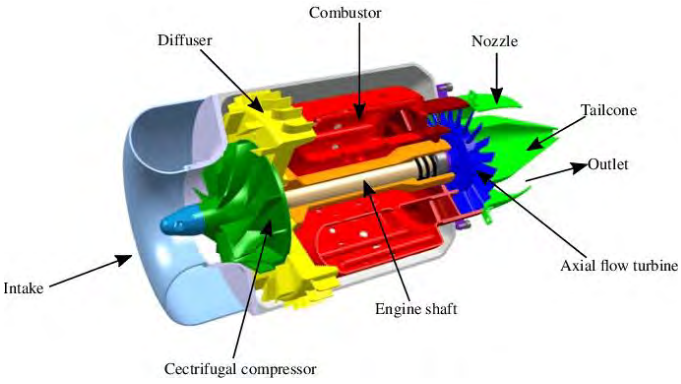

Micro gas turbine engine (researchgate.net)

b) structure

Figure 1 The schematic diagram of the KJ66 MGT engine structure

The engine has been the subject of numerous studies on its components and overall performance, with several researchers dedicating time to investigate (Xiang and Schlüter et al., 2017; Xu and Yan et al., 2022; Yang and Wu et al., 2022). Additionally, experimental data on thrust, rotational speed, and specific fuel consumption is available in Ref. (Schreckling, 2005) and will be used for comparative analysis in the next section of the paper. It is noteworthy that all of these performance metrics were obtained under sea-level conditions based on the International Standard Atmosphere (ISA). Table 1 presents a comprehensive list of the design parameters and performance characteristics of the KJ66 MGT.

Table 1 Design parameters and performance characteristics of the KJ66 MGT

Parameters	Values
Maximum thrust [N]	84.5
Maximum permitted rotational velocity [RPM]	120,000

Pressure ratio [-]	2.15
Mass flow [kg/s]	0.23
Exhaust gas temperature [K]	853.15
Recommended maximum thrust [N]	75
Rotational speed at recommended maximum thrust [RPM]	114,700

Component level model

The component-level model is a simulation approach for aeroengines that does not involve the use of computational fluid dynamics (CFD). Instead, it relies on a set of equations and algorithms to represent the performance of each component within the engine. The model breaks down the engine into its main components, such as the compressor, turbine, and combustion chamber and simulates each component's behavior based on its design parameters, operating conditions, and performance characteristics. The model uses a combination of theoretical equations, empirical data, and experimental results to predict the overall performance of the engine. The component-level model allows for a rapid evaluation of the engine's performance under various operating conditions and can aid in the optimization of engine design and operation.

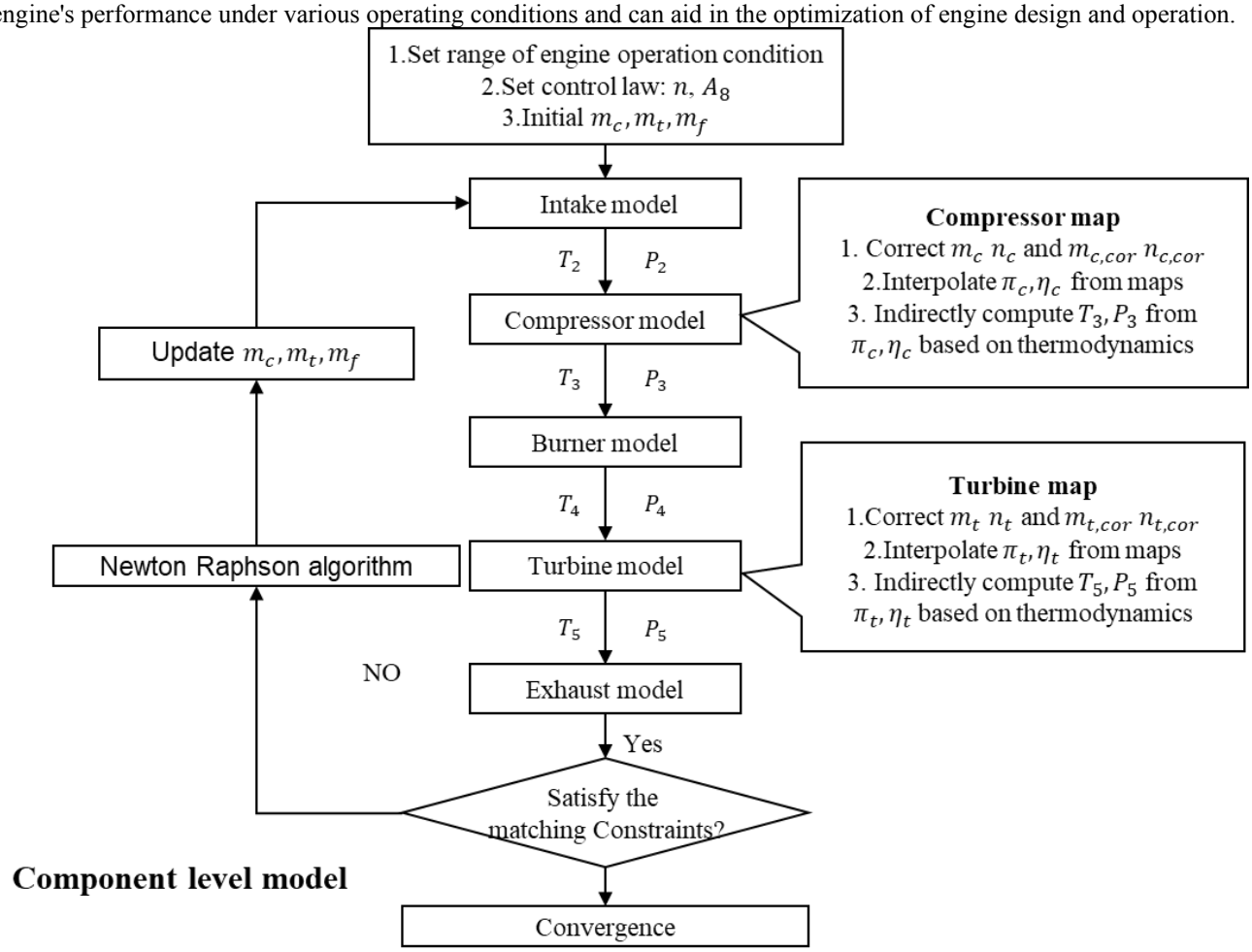

Figure 2 The flowchart of the CLM for KJ66 MGT

In this paper, the authors have developed a CLM that is derived from the fundamental principles of conservation of mass flow, pressure balance, and power balance. These equations are used to establish the cooperation equations that represent the relationships between the various components of the engine. The CLM focuses on simulating the behavior of the compressor and turbine, which are critical components of the engine. The corresponding cooperation equations of CLM are established, including the relative error of the compressor and turbine mass flow, turbine and exhaust mass flow, and compressor and turbine power in the cooperation equations.

First, the conservation of mass flow between compressor and turbine without consideration of air bleed:

$$e_1 = f_{map,1} = \left(m_c + m_f - m_t\right)/m_t \quad (1)$$

where m_t means the turbine gas mass flow interpolated and corrected from the turbine characteristic map; m_c means the compressor air mass flow interpolated and corrected from the compressor characteristic map; m_f means the aviation kerosene mass flow calculated by the 0D empirical burner model; $f_{map,1}$ represent the first equilibrium equation incorporating characteristic maps; e_1 means the residual of the first equilibrium equation.

Second, the conservation of mass flow between the turbine and exhaust:

$$e_2 = f_{map,2} = (m_t - m_e)/m_e \quad (2)$$

where m_e means the exhaust gas mass flow is determined by the 0D empirical exhaust model; $f_{map,2}$ represent the second equilibrium equation incorporating characteristic maps; e_2 means the residual of the second equilibrium equation.

Third, the power balance between compressor and turbine without consideration of power extraction:

$$e_3 = f_{map,3} = \frac{(PW_c - PW_t)}{PW_t} \quad (3)$$

where PW_c and PW_t mean the compressor and turbine power calculated by compressor and turbine 0D thermodynamic models, respectively; $f_{map,3}$ represent the third equilibrium equation incorporating characteristic maps; e_3 means the residual of the third equilibrium equation.

The CLM relies on the characteristic maps of the compressor and turbine, which are typically obtained through extensive experimental testing or numerical simulation. These maps describe the behavior of the components as a function of various operating parameters, such as rotational speed and pressure ratio. In the CLM model, these maps are used to calculate the mass flow and power of the components, which are then used to determine the overall performance of the engine. The characteristic maps are expressed as Eq. 4) and include parameters where π means pressure ratio, η means isotropic efficiency, n_{cor} means corrected rotational speed, and m_{cor} means corrected mass flow. It is important to note that these maps are typically generated under standard operating conditions, known as the International Standard Atmosphere (ISA), and may require corrections under different operating conditions. The CLM model takes these corrections into account to ensure accurate performance predictions under real conditions.

$$\begin{cases} (\pi_c, \eta_c) = f_{map}(n_{cor,c}, m_{cor,c}) \\ (\pi_t, \eta_t) = f_{map}(n_{cor,t}, m_{cor,t}) \end{cases} \quad (4)$$

The flowchart of the CLM for KJ66 MGT is depicted in Figure 2, which consists of six distinct modules. The first module is the intake model, which calculates the intake thermodynamic parameters based on the given flight conditions. The compressor and turbine modules, on the other hand, interpolate the component characteristic parameters using the characteristic maps and calculate thermodynamic parameters based on them. The burner module determines the burner characteristics through empirical expressions, while the exhaust module computes thermodynamic parameters based on the state of the exhaust. Finally, the Newton-Raphson solver uses an iterative approach to solve the cooperation equations.

In the original cooperation equations of KJ66 MGT, there were three independent variables for the components. However, by replacing the characteristic maps with those obtained from 3D CFD models, it became possible to choose the independent variables of the cooperation equations as real mass flow directly instead of the corrected mass flow. This allowed for a direct exchange of parameters between the CLM and CFD models without the need for any transformation. Therefore, in the modified cooperation equations, as shown in Eq. 8), the mass flow of the compressor m_c, turbine m_t, and fuel m_f were chosen as the independent variables. By expressing the cooperation equations as a function of these independent variables, the exchange of parameters between the CLM and CFD models was more efficient and direct.

3D CFD models of rotating components

The 3D CFD models of the compressor and turbine in the fully coupled zooming method were utilized through ANSYS CFX. To verify the reliability of the 3D simulation results, Table 2 presents various grid configurations (serial numbers 1-6) along with the corresponding grid numbers for the 3D models. Notably, the mesh number per blade passage of both impellor and duffuser was approximately 700,000, and the mesh number per blade passage of both vane and rotor was around 750,000, approximately. This indicates that the characteristic parameters of these components did not change significantly with increasing mesh count. To reduce computational costs, a single-blade passage was used for the impellor, diffuser, turbine vane, and rotor. Further information about the chosen mesh can be found in Table 3, and the 3D meshes for the compressor and turbine CFD models can be seen in Figure 3.

Table 2 various grid configurations of component

Serial nunber	Compressor Mesh level	Efficiency Relative Error	Massflow Relative Error	Turbine Mesh level	Efficiency Relative Error	Pressure Ratio Relative Error
1	250,000	0.58%	3.00%	250,000	1.06%	1.32%
2	350,000	0.32%	2.32%	350,000	0.41%	0.83%
3	500,000	0.22%	1.49%	500,000	0.51%	0.78%
4	700,000	0.06%	0.73%	750,000	0.21%	0.59%
5	1,300,000	0.05%	0.32%	1,250,000	0.18%	0.58%
6	1,650,000	Reference	Reference	1,750,000	Reference	Reference

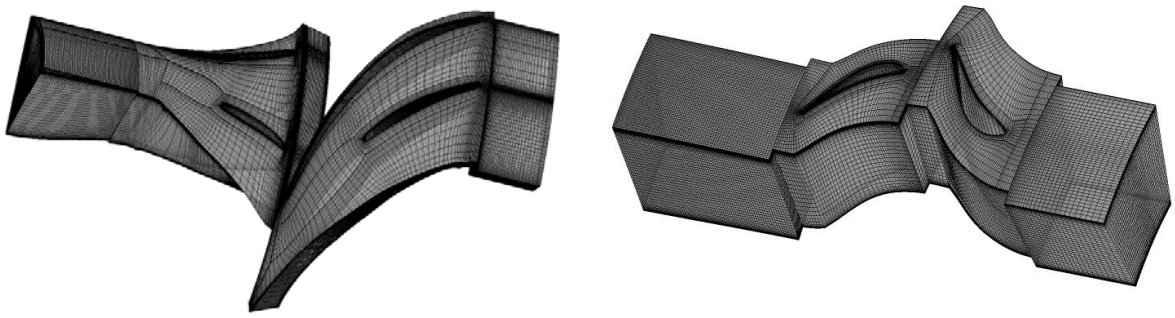

Figure 3 3D meshes for the compressor and turbine CFD models

Table 3 Selected mesh information of component

Component	Compressor		Turbine	
Zone	Impellor	Diffuser	Vane	Rotor
Geometry Periodicity	6	12	18	24
Mesh type	Hexahedra	Hexahedra	Hexahedra	Hexahedra
Elements	650 000	620 000	720 000	695 000

The steady compressible RANS equations were solved using a finite control volume method for discretization, with an overall accuracy of the second order. At the rotor-stator interface of the computational domain, a mixing plane approach was employed with a stage average velocity constraint, using different reference frames. To model turbulence, the k-ε turbulent model with scalable wall functions was used according the previous verification (Briones and Sykes et al., 2020; Briones and Caswell et al., 2021). The y-plus near the wall met the requirement for calculating the boundary velocity with scalable wall functions. Overall, these methods and models were chosen to ensure accurate and reliable numerical simulations for the study. The inlet boundary of the compressor and turbine was the flow direction, total pressure, and total temperature; and the outlet boundary was the mass flow or static pressure. The rotational speed also was input to CFD models. To balance computational costs, a single-blade passage was used for the impellor, diffuser, turbine vane, and rotor. After these, the 3D steady numerical simulation of the above two components are solved, where the equations are solved using the steady Navier-Stokes equations, the three laws of mass conservation, momentum conservation, and energy conservation are applied to gas clusters to obtain the governing equation of compressible Newtonian fluid——Navier-Stokes equations, whose form in the relative cylindrical coordinate system is shown in Eq. 5).

$$\frac{\partial U}{\partial t}+\frac{\partial (E-V_x)}{\partial x}+\frac{\partial (F-V_s)}{r\,\partial \theta}+\frac{\partial r(G-V_r)}{r\,\partial r}=S \tag{5}$$

$$U=\begin{bmatrix}\rho\\ \rho u\\ \rho v_\theta\\ \rho v_r\\ \rho E\end{bmatrix}\ E=\begin{bmatrix}\rho u\\ \rho uu+p\\ \rho v_\theta u\\ \rho v_r u\\ \rho H u\end{bmatrix}\ F=\begin{bmatrix}\rho v_\theta\\ \rho u v_\theta\\ \rho v_\theta v_\theta+p\\ \rho v_r v_\theta\\ \rho H v_\theta\end{bmatrix}\ G=\begin{bmatrix}\rho v_r\\ \rho u v_r\\ \rho v_\theta v_r\\ \rho v_r v_r+p\\ \rho H v_r\end{bmatrix}$$

$$V_x=\begin{bmatrix}\mathbf{0}\\ \tau_x\\ \tau_{\theta x}\\ \tau_n\\ u\tau_x+v_\theta\tau_\alpha+v_r\tau_x-q_x\end{bmatrix}\ V_\theta=\begin{bmatrix}0\\ \tau_{x\theta}\\ \tau_{\theta\theta}\\ \tau_{\theta\theta}\\ \tau_{r\theta}\\ u\tau_{x\theta}+v_\theta\tau_{\theta\theta}+v_r\tau_{r\theta}-q_\theta\end{bmatrix}$$

$$V_r=\begin{bmatrix}\mathbf{0}\\ \tau_x\\ \tau_s\\ \tau_r\\ u\tau_x+v_s\tau_s+v_r\tau_r-q_r\end{bmatrix}\ S=\begin{bmatrix}0\\ 0\\ \frac{-\rho v_\theta v_r+\tau_{\theta r}}{r}\\ r\\ \frac{\rho v_\theta v_\theta+p-\tau_{\theta\theta}}{r}\end{bmatrix}$$

Moreover, the outlet total temperature and pressure of the compressor and turbine are directly captured by mass flow averaged using CFD models. Additionally, the power of the compressor and turbine is directly obtained by numerical integration using CFD models. This notably differs from the component-level model, where the outlet total temperature, pressure, and power of the compressor and turbine are indirectly calculated from the efficiency and pressure ratio according to the thermodynamics principle. In summary, the high-fidelity model of the compressor and turbine can be expressed as Eqs. 6) and 7).

$$\begin{cases}(T_3,p_3)=f_{CFD,c}(n,m_c)\\ (T_5,p_5)=f_{CFD,t}(n,m_t)\end{cases} \tag{6}$$

$$\begin{cases} L = \left(\int_S \left(\vec{r} \times (\bar{\tau} \cdot \hat{n}) \right) dS \right) \cdot \hat{a} \\ PW = Ln \end{cases} \quad 7)$$

where L is the torque of the rotating parts of the compressor or turbine, S is the surface comprising all rotating parts, $\bar{\tau}$ is the total stress tensor, $\hat{n}$ is a unit vector normal to the surface, $\vec{r}$ is the position vector, and $\hat{a}$ is a unit vector parallel to the axis of rotation, PW is the power of the compressor or turbine.

Fully coupled zooming method

In the original cooperation equations of KJ66 MGT, there were three independent variables for the components. However, by replacing the characteristic maps with those obtained from 3D CFD models, it became possible to choose the independent variables of the cooperation equations as real mass flow directly instead of the corrected mass flow. This allowed for a direct exchange of parameters between the CLM and CFD models without the need for any transformation. Therefore, in the modified cooperation equations, as shown in Eq. 8), the mass flow of the compressor m_c, turbine m_t, and fuel m_f were chosen as the independent variables. By expressing the cooperation equations as a function of these independent variables, the exchange of parameters between the CLM and CFD models was more efficient and direct.

$$\boldsymbol{F}_{CFD}(\boldsymbol{X}) = \begin{cases} f_{CFD,1}(m_c, m_t, m_f) = e_1 \\ f_{CFD,2}(m_c, m_t, m_f) = e_2 \\ f_{CFD,3}(m_c, m_t, m_f) = e_3 \end{cases} \quad 8)$$

For simplicity, the cooperation equations can be expressed as $\boldsymbol{F}(\boldsymbol{X}) = \boldsymbol{E}$, where $\boldsymbol{E} = [e_1, e_2, e_3]$, and the independent variables (m_c, m_t, m_f) are denoted as $\boldsymbol{X} = [\mathrm{x}_1, \mathrm{x}_2, \mathrm{x}_3]$. So the Newton-Raphson method can be expressed as Eqs. 9) and 10).

$$\boldsymbol{X}^{(i+1)} = \boldsymbol{X}^{(i)} - \left(\boldsymbol{J}^{(i)}\right)^{-1} \boldsymbol{F}^{(i)} \quad 9)$$

$$\boldsymbol{J}^{(i)} = \boldsymbol{J}(\boldsymbol{X}) = \frac{\partial \boldsymbol{E}}{\partial \boldsymbol{X}} = \left(\nabla \boldsymbol{E}(\boldsymbol{X})\right)^T = \begin{bmatrix} \frac{\partial e_1}{\partial x_1} & \frac{\partial e_1}{\partial x_2} & \frac{\partial e_1}{\partial x_3} \\ \frac{\partial e_2}{\partial x_1} & \frac{\partial e_2}{\partial x_2} & \frac{\partial e_2}{\partial x_3} \\ \frac{\partial e_3}{\partial x_1} & \frac{\partial e_3}{\partial x_2} & \frac{\partial e_3}{\partial x_3} \end{bmatrix} \quad 10)$$

The Newton-Raphson method iteratively solves the cooperation equations until the accuracy standard $\left\|\boldsymbol{E}^{(i)}\right\|_2 < \sigma$ is satisfied, $\left\|\boldsymbol{E}^{(i)}\right\|_2$ is shown in Eq. 11).

$$\left\|\boldsymbol{E}^{(i)}\right\|_2 = \sqrt{\left(e_1^i\right)^2 + \left(e_2^i\right)^2 + \left(e_3^i\right)^2} \quad 11)$$

In summary, the fully coupled zooming method is that it eliminates the need for characteristic maps and the correction between real conditions and ISA. This means that the corrected mass flow and rotational speed are not required, and the characteristics of the compressor and turbine can be expressed directly. In contrast, the CLM method indirectly computes the outlet total temperature and pressure of the compressor and turbine from efficiency and pressure ratio according to thermodynamics.

The schematic of the fully coupled zooming model built for KJ66 in this paper is shown in Figure 4, which realizes the zooming of the dual rotating components, including the compressor and turbine. The 0D components model of the intake, burner and exhaust are built by SIMULINK/MATLAB, which are the same in the fully coupled zooming model and the CLM. And the component characteristic parameters of the compressor and turbine are obtained by self-programmed CFX macro scripts. The 3D CFD models of the compressor and turbine are directly embedded in the corresponding engine SIMULINK module using self-programmed Python communication scripts, which is significantly different from the interpolation-based 0D component module of the compressor and turbine in CLM. The Newton-Raphson solver iteratively solves the cooperation equations until the error criteria are satisfied.

In detail, the fully coupled zooming model used in this study comprises three main modules, namely, 0D component modules, 3D CFD models, and a cycle solving module. The 0D component modules calculate the characteristics of non-rotating components such as the intake, burner, and exhaust using existing empirical correlations. On the other hand, the 3D CFD models are used to simulate and extract the characteristic parameters of the compressor and turbine. To transfer the parameters from the 0D component module to the corresponding boundary conditions of the 3D CFD model, a uniform distribution is used, including the compressor and turbine total inlet temperature, and total inlet pressure. Furthermore, the 3D distribution of interface parameters simulated by the 3D CFD model is directly transferred to the 0D thermodynamic parameters through mass flow averaging. The 0D component module and the 3D CFD model are run sequentially according

to the physical assembly sequence. The cycle solving module calculates the errors, and then iteratively solves the cooperation equations using the Newton-Raphson method until the error criteria are satisfied.

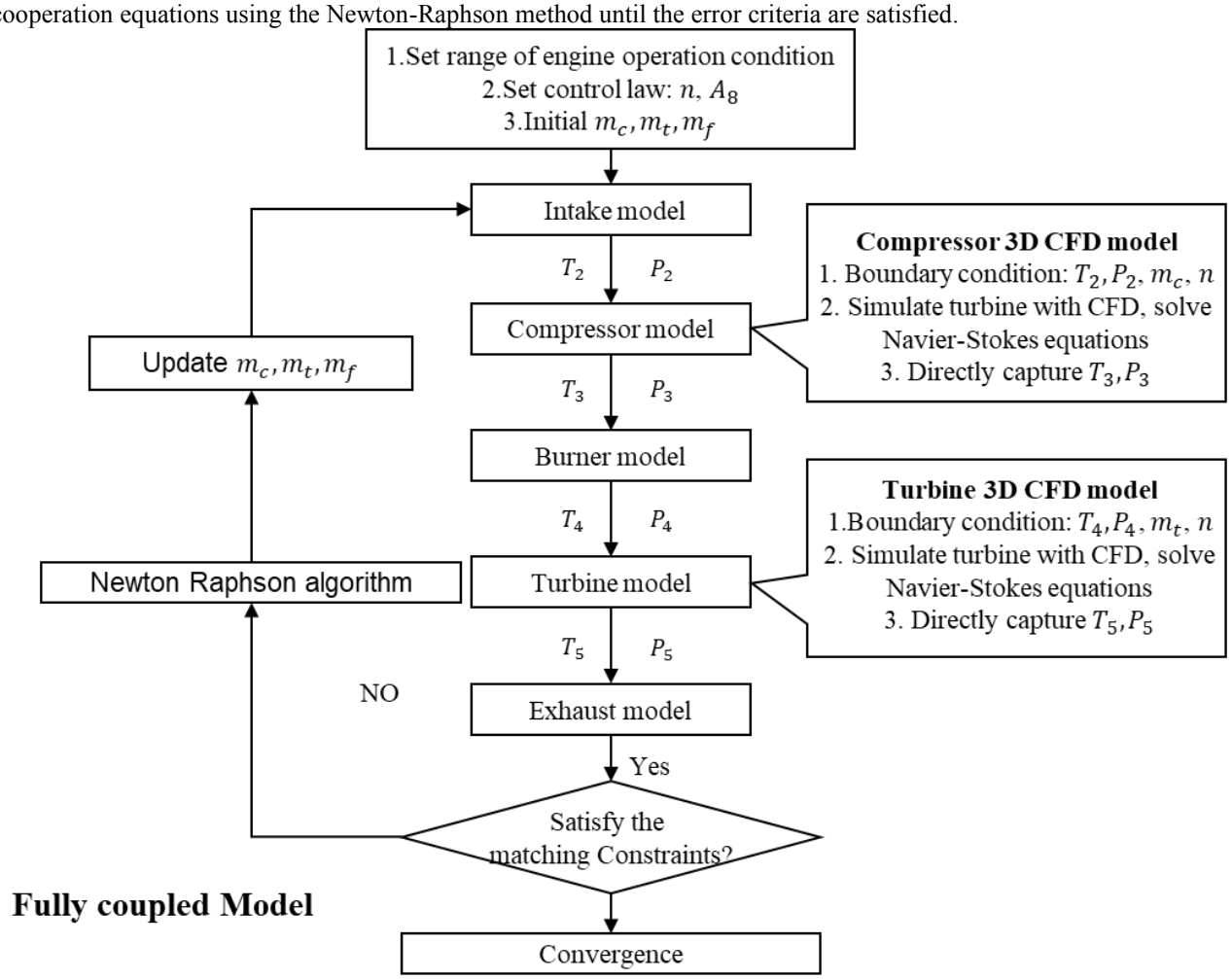

Figure 4 The schematic of the fully coupled zooming model built for KJ66

RESULTS AND DISCUSSION

The effectiveness of the fully coupled zooming method was evaluated by simulating the throttle characteristics of the KJ66 MGT at a wide range of off-design conditions. To achieve the throttle characteristics at ISA, several rotational speeds ranging from 60 000 to 120 000 RPM were selected to calculate the thrust, specific fuel consumption (sfc), and other parameters. The experimental data provided in Ref. (Schreckling, 2005) were used for comparison.

To quantify the error between the numerical simulation results and the experimental data, the global error e_a was employed, which is a commonly used metric in engineering simulations. The global error is defined as the mean of the absolute differences between the predicted and measured data points, normalized by the average of the measured data. It is calculated using the following Eq. 12), where n is the number of test data points, p_i denotes the ith predicted data, and p_{mi} denotes the ith measurement data.

$$e_a = \frac{1}{n}\sum_{i=1}^{n}\left|\frac{p_i - p_{mi}}{p_{mi}}\right| \quad 12)$$

Table 4 The global error of the throttle characteristic

Parameters	$Thrust$	T_5	T_3	sfc
CLM	6.639%	5.484%	7.486%	13.969%
Fully coupled	4.078%	4.535%	6.196%	9.286%

Figure 5 presents a comparative analysis of the experimental and numerical simulation results obtained through the fully coupled and CLM methods. The results indicate that both methods demonstrate a high level of prediction accuracy for parameters π_c, thrust, and T_3, especially the fully coupled zooming method has higher prediction accuracy (Figure 5 see (a), (b) and Table 4).

The figure also highlights the significant differences between the two methods predictions for T_5 and sfc. Notably, the prediction accuracy of T_5 calculated by the CLM method is low, with the global error reaching 5.484%, the fully coupled zooming method reduces the error to 4.535%, thus offering a better prediction accuracy (see Figure 5 (c) and Table 4), the fully coupled method also captured the increasing trend at the low-speed region, which the CLM method did not. Additionally, the prediction accuracy of sfc calculated by the CLM remains low, with a global error of about 14%, whereas the fully coupled zooming method delivers a significantly better prediction accuracy with a global error of around 9.5% (see Figure 5 (d) and Table 4). In summary, the fully coupled zooming method offers a substantial improvement in accuracy, particularly for off-design points in the low rational speed region. Particularly it gave a sufficiently high accuracy in the low rotational speed region and a slightly low accuracy in the high rotational speed region.

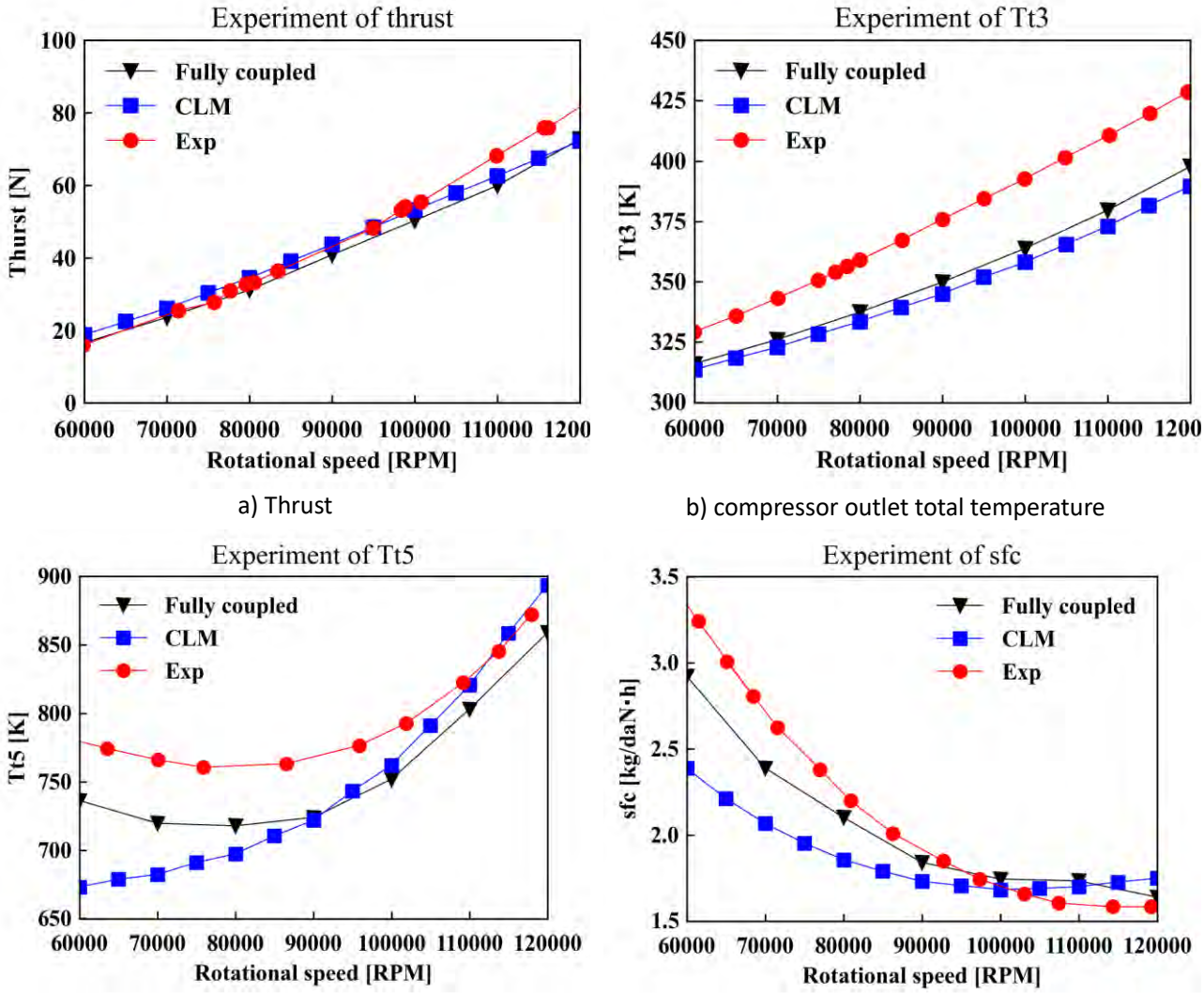

a) Thrust

b) compressor outlet total temperature

c) Turbine outlet total temperature

d) Specific fuel consumption

Figure 5 Comparison of throttle characteristics of KJ66 MGT

The accuracy of component-level model are primarily dependent on the characteristic maps, which are generated under standard operating condition corresponding to the design point. Due to Due to their inability to capture detailed component information and real operating conditions, the characteristic maps can introduce some errors, necessitating extensive modification and correction through experiment and expert knowledge, especaily in the off-desigin point. In contrast, the fully coupled method operates without the need for characteristic maps. Moreover, each iterative solution of the equilibrium equations originates from CFD numerical simulations conducted under actual operating conditions. This intrinsic advantage results in heightened accuracy, even in off-design scenarios such as the low-speed region. Consequently, the fully coupled method exhibits remarkable accuracy, particularly in off-design conditions.

While the total number of iterations in the overall performance simulation serves as a significant indicator of overall convergence behavior, it does not necessarily directly correlate with the total simulation time. For instance, a single performance run of a component-level model achieves convergence within a relatively brief span of approximately 0.1 seconds Therefore, the primary determinant of simulation duration is the creation of characteristic maps through CFD

simulations. Consequently, the overall simulation time for a specific speed line within these maps is greatly influenced by the associated CFD simulations, each requiring 12 runs and contributing to an aggregate simulation time of 12 hours. However, Converging one operational point within the fully coupled model eventually took around 24 hours, encompassing 12 iterations. Nonetheless, the improved accuracy of the fully coupled model at low speed region justifies the added computational cost.

After analyzing the results, it was found that the fully coupled zooming method outperformed the CLM method in terms of accuracy. In addition, the fully coupled method also provided a more comprehensive understanding of the complex flow characteristics within the engine, as shown in Figure 6. This figure illustrates the detailed static pressure distribution of the compressor and turbine, which cannot be captured by the CLM method. Therefore, the fully coupled method is not only more accurate but also provides additional insights into the internal flow detail of the engine. This information is crucial for optimizing the engine's design and improving its performance. In summary, the CWCFD method offers a higher global accuracy of throttle characteristics than other methods, when averaged over the whole rotational speed region. The accuracy at low rotational speeds is sufficiently higher than other methods, and the accuracy at high rotational speeds is lower.

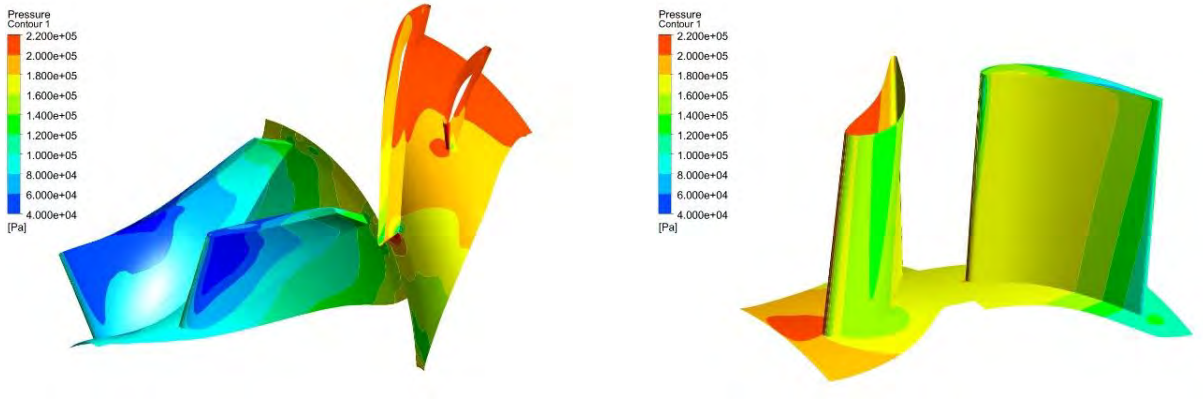

a) Compressor b) Turbine

Figure 6 Static pressure distribution of rotating components

CONCLUSIONS

A fully coupled numerical zooming method was developed in this paper, which directly exchanges mass flow between CFD and CLM. The fully coupled zooming method is implemented by embedding multiple 3D CFD models of compressor and turbine (coaxial rotating), instead of the corresponding characteristic maps, into a CLM, and it was applied to the simulation of the KJ66 MGT. The throttle characteristics including a wide range of off-design points are simulated. The fully coupled zooming method is compared with the traditional CLM method. Finally, the experimental data of the ground test are carried out to verify the effectiveness of the zooming methods. The results were analyzed in detail, and the performance of the fully coupled zooming method was found to be superior to the CLM method in terms of accuracy. However, the improved accuracy of the approach at low speed region justifies the added computational cost.

It is worth noting that the fully coupled zooming method eliminates the need for characteristic maps and correction between real conditions and ISA. The replacement of corrected mass flow and corrected rotational speed with the actual mass flow and rotational speed avoids some computation errors from correction. Moreover, it allows the option of selecting independent variables of the cooperation equations as mass flow rather than the corrected mass flow, which simplifies the exchange of parameters between CLM and CFD models. The results suggest that the fully coupled zooming method is a promising alternative to future aeroengine design and optimization.

NOMENCLATURE

Notation

P	Total pressure
T	Total temperature
P_s	Static pressure
p_i	Predicted data
p_{mi}	Measured data
n	Rotational speed
sfc	Specific fuel consumption
m	Mass flow

$\boldsymbol{E}, e$	Error
$\boldsymbol{J}$	Jacobi matrix
$\boldsymbol{F}$	Cooperation functions
L	Power
π	Pressure ratio
η	Isentropic efficiency
n_{cor}	Corrected rotational speed
m_{cor}	Corrected mass flow
A_8	Exhaust Area

Superscripts/Subscripts:

0	Ambient
1	Inlet of the intake
2	Inlet of the compressor
3	Inlet of the burner
4	Inlet of the turbine
5	Outlet of the turbine
8	Outlet of the exhaust
c	Compressor
b	Burner
t	Turbine
e	Exhaust
f	Fuel
cor	Parameter at ISA

ACKNOWLEDGMENTS

This research was funded by the Science and Technology Innovation Committee Foundation of Shenzhen, Grant No. JCYJ20200109141403840 and Grant No. ZDSYS20220527171405012, and the National Natural Science Foundation of China (NSFC), Grant No.52106045.

References:

Allison, D. L. and E. J. Alyanak (2014). Development of Installed Propulsion Performance Model for High-Performance Aircraft Conceptual Design.

Bala, A. (2007). Poly-dimensional gas turbine system modelling and simulation, Cranfield University.

Briones, A. M. and A. W. Caswell, et al. (2021). "Fully Coupled Turbojet Engine Computational Fluid Dynamics Simulations and Cycle Analyses Along the Equilibrium Running Line." J. Eng. Gas Turbines Power **143** (6).
Briones, A. M. and A. W. Caswell, et al. (2021). "Fully Coupled Turbojet Engine Computational Fluid Dynamics Simulations and Cycle Analyses Along the Equilibrium Running Line." Journal of Engineering for Gas Turbines and Power **143** (6).
Briones, A. and J. Sykes, et al. (2020). Steady-state CFD Simulations of a Small-scale Turbojet Engine from Idle to Cruise Conditions. AIAA Scitech 2020 Forum.
Connolly, J. W. and D. J. Friedlander, et al. (2014). Computational fluid dynamics modeling of a supersonic nozzle and integration into a variable cycle engine model.
Fu, S. and Z. Li, et al. (2021). "Integration of high-fidelity model of forward variable area bypass injector into zero-dimensional variable cycle engine model." Chinese Journal of Aeronautics **34** (8): 1-15.
Hao, X. and L. Sun, et al. (2022). "Off-Design Performance of 9F Gas Turbine Based on gPROMs and BP Neural Network Model." Journal of Thermal Science **31** (1): 261-272.
JIA, L. and Y. CHEN, et al. (2021). "Designing method of acceleration and deceleration control schedule for variable cycle engine." Chinese Journal of Aeronautics **34** (5): 27-38.
Jia, Z. and H. Tang, et al. (2022). "Research on the volume-based fully coupled method of the multi-fidelity engine simulation." Aerospace Science and Technology **123**: 107429.
Klein, C. and S. Reitenbach, et al. (2017). A fully coupled approach for the integration of 3D-CFD component simulation in overall engine performance analysis. ASME GT 2017-63591, American Society of Mechanical Engineers.
Lytle, J. (2006). Multi-fidelity simulations of air breathing propulsion systems.
Medic, G. and D. You, et al. (2007). Integrated computations of an entire jet engine.
Pachidis, V. and P. Pilidis, et al. (2006). "A fully integrated approach to component zooming using computational fluid dynamics." Proceedings of the Institution of Mechanical Engineers, Part G: Journal of Aerospace Engineering.
Pachidis, V. and P. Pilidis, et al. (2007). "A comparison of component zooming simulation strategies using streamline curvature." Proceedings of the Institution of Mechanical Engineers, Part G: Journal of Aerospace Engineering **221** (1): 1-15.
Pachidis, V. and P. Pilidis, et al. (2007). "A de-coupled approach to component high-fidelity analysis using computational fluid dynamics." Proceedings of the Institution of Mechanical Engineers, Part G: Journal of Aerospace Engineering **221** (1): 105-113.
Pang, S. and Q. Li, et al. (2020). "A hybrid onboard adaptive model for aero-engine parameter prediction." Aerospace Science and Technology **105**: 105951.
Pilet, J. and J. C. Lecordix, et al. (2011). Towards a fully coupled component zooming approach in engine performance simulation. ASME GT 2011-46320.
Schlu Ter, J. R. and S. Apte, et al. (2006). Unsteady CFD simulation of an entire gas turbine high-spool.
Schreckling, K. (2005). Home Built Model Turbines. Worcestershire, UK, Traplet Publications Ltd.
Wang, Z. and J. Zhang, et al. (2023). "Effect of air properties on a twin-shaft turbofan engine performance during start-up." Applied Thermal Engineering **218**: 119387.
Xiang, J. and J. U. Schlüter, et al. (2017). "Study of KJ-66 micro gas turbine compressor: Steady and unsteady Reynolds-averaged Navier – Stokes approach." Proceedings of the Institution of Mechanical Engineers, Part G: Journal of Aerospace Engineering **231** (5): 904-917.
Xu, Y. and C. Yan, et al. (2022). "Analysis of discrepancies between 3-D coupled and uncoupled schemes based on CFD in full engine simulation." Aerospace Science and Technology **131**: 107978.
Yang, C. and H. Wu, et al. (2022). "Full-engine simulation of micro gas turbine based on time-marching throughflow method." Applied Thermal Engineering **217**: 119213.
ZHENG, X. and H. ZENG, et al. (2023). "Numerical simulation method of surge experiments on gas turbine engines." Chinese Journal of Aeronautics **36** (3): 107-120.
ZHOU, X. and F. LU, et al. (2019). "Fault diagnosis based on measurement reconstruction of HPT exit pressure for turbofan engine." Chinese Journal of Aeronautics **32** (5): 1156-1170.
Zhuang, L. and G. Xu, et al. (2023). "Study on performance and mechanisms of a novel integrated model with Power & Thermal Management system and turbofan engine." Applied Thermal Engineering **219**: 119481.